Anomalous conduction and second sound in the Fermi-Pasta-Ulam-Tsingou chain: wave-turbulence approach

Francesco De Vita,[1] Giovanni Dematteis,[2] Raffaele Mazzilli,[3] Davide Proment,[4] Yuri V. Lvov,[2] and Miguel Onorato[5, 6]

[1]*DMMM, Politecnico di Bari, Via Re David 200, Bari, 70125, Italy*
[2]*Department of Mathematical Sciences, Rensselaer Polytechnic Institute, Troy, NY (US)*
[3]*Max-Planck-Institut für Festkörperforschung, 70569 Stuttgart, Germany*
[4]*School of Mathematics, University of East Anglia,*
Norwich Research Park, NR4 7TJ Norwich, United Kingdom
[5]*Dipartimento di Fisica, Università di Torino, Via P. Giuria, 1 - Torino, 10125, Italy*
[6]*INFN, Sezione di Torino, Via P. Giuria, 1 - Torino, 10125, Italy*
(Dated: March 17, 2022)

One-dimensional particle chains are fundamental models to explain anomalous thermal conduction in low-dimensional solids like nanotubes and nanowires. In these systems the thermal energy is carried by phonons, i.e. propagating lattice oscillations that interact via nonlinear resonance. The average energy transfer between the phonons is described by the wave kinetic equation (WKE), derived directly from the microscopic dynamics. Here, we use the spatially nonhomogeneous WKE of the prototypical β−Fermi-Pasta-Ulam-Tsingou (FPUT) model, equipped with thermostats able to set different temperatures at the two ends. Our main findings are as follows: (i) The anomalous scaling of the conductivity with the system size, in close agreement with the known results from the microscopic dynamics, is due to a nontrivial interplay between high and low wavenumbers. (ii) The high-wavenumber phonons relax to local thermodynamic equilibrium transporting energy diffusively, *à la Fourier*. (iii) The low-wavenumber phonons are nearly noninteracting and transfer energy ballistically; this latter phenomenon is the analogous of the second sound emission, observed for example in superfluids.

That heat conduction in three-dimensional macroscopic solids is described effectively by Fourier's law has been known for two centuries [1]. This law establishes the existence of a size-independent *property of the material*, the heat conductivity $\mathcal{K}$, as a finite proportionality constant between the heat flux and its driving *thermodynamic force*, the temperature gradient [2]. In low-dimensional solids this proportionality may break down and size-dependent conduction effects arise. One-dimensional (1D) particle chains characterized by harmonic potential have a conductivity proportional to the chain length L, that is $\mathcal{K} \propto L^1$ [3]. The lattice excitations propagate unperturbed as non-interacting wave packets; this implies absence of relaxation. Therefore, energy is transported by advection (or *ballistically* [4]), rather than by diffusion as prescribed by Fourier's law. Intermediate behaviors in which $\mathcal{K} \propto L^\alpha$, with $0 < \alpha < 1$, are observed both in numerical simulations of more realistic particle chains [5, 6] and in experiments involving nearly 1D systems such as carbon nanotubes and silicon nanowires [7–12]. This type of transport, neither diffusive nor ballistic, is referred to as *anomalous* and its investigation, motivated by the relevance of the widespread technological applications, has generated a large body of literature in the last two decades [13].

A minimal model displaying anomalous transport is the Fermi-Pasta-Ulam-Tsingou (FPUT) chain [14, 15], in which a cubic (α−FPUT) or quartic (β−FPUT) anharmonic term is added to the harmonic potential. Physically, this term represents the lowest-order nonlinear correction to the linearized harmonic system, in a power-law expansion of the potential around the equilibrium point.

Weak nonlinearity plays a crucial role in the derivation of the so-called *phonon Boltzmann equation*, or *wave kinetic equation* (WKE) [16–20]. The WKE is the statistical closure of the deterministic equations of motion, for the *spectral action density* $n(k, t)$, *i.e.* the second moment of the random wavefield in Fourier space; $n(k, t)$ is related to the spectral energy density $e(k)$ via $e(k) = \omega(k)n(k)$, where $\omega(k)$ is the linear dispersion relation. The WKE contains the statistical description of the action/energy transfers between the various wave modes. These transfers are mediated by the *collision integral*, which incorporates the nonlinear terms in the WKE as wave-wave resonant interactions between the eigenstates of the harmonic chain, i.e. the linear waves. The time scales of the resonant transfers, the *kinetic time scales*, are much longer than the linear time scale of wave propagation, where the scale separation is tied to the smallness of the nonlinearity. For β−FPUT in the thermodynamic limit (large system), the quartic term in the potential yields a collision integral encoding 4−wave resonant interactions [21–23] that exchange energy between quartets of wave modes and, ultimately, lead to relaxation over the kinetic time scales [24].

A kinetic interpretation of the numerically observed anomalous exponent $\alpha \simeq 0.4$ [25] in the β−FPUT system was proposed in [26] and given rigorous justification in [27, 28]. The result is based on an asymptotic approximation of the collision integral for the *acoustic modes*, as $k \to 0$, and on a subsequent heuristic cut-off applied to the linear-response Kubo integration of the correlation function [5]. In [29], an analogous asymptotic result was exploited to identify a critical scale k_c determining a sep-

aration between two sets of modes: those with $|k| < k_c$ essentially behave as ballistic modes in an harmonic chain, as they lack a sufficient level of interaction; the modes with $|k| > k_c$ are diffusive and relax locally to the expected Fourier profile. In this interpretation, the anomalous exponent is due to how the separation between the two sets scales with the chain length, given by a certain function $k_c(L)$. Rather than from an anomalous type of diffusion (such as fractionary diffusion), the anomalous transport properties thus arise from a coexistence of regular diffusion and advective effects that persist on macroscopic scales due to the properties of the collision integral.

Here, we go beyond the asymptotic result for the acoustic modes and fully exploit the mesoscopic picture, by direct numerical integration in time of the spatially-nonhomogeneous WKE associated with the β–FPUT model. We show that the first-principle description of the WKE is able to reproduce accurately the anomalous transport properties observed in the direct numerical simulations of the microscopic dynamics [13]. We also confirm results previously conjectured on the separation between ballistic modes and diffusive modes [29], and characterize the respective transport coefficients. Finally, we exploit the higher-level, and computationally much cheaper picture of the WKE, to investigate in detail the local relaxation properties of the different modes.

MODEL

To simulate thermal energy transfers through a one-dimensional particle chain we solve the following space-dependent WKE associated with the β–FPUT model in the thermodynamic limit [24], for the spectral action density $n_k = n(x, k, t)$ [19, 30, 31]

$$\frac{\partial n_k}{\partial t} + v_k \frac{\partial n_k}{\partial x} = \mathcal{I}_k. \tag{1}$$

We denote by $x \in [0, L]$, $k \in [0, 2\pi)$ and $t > 0$ the (macroscopic) physical space, the Fourier space and the time variables, respectively. The second term at the LHS of (1) represents the advection of n_k due to spatial inhomogeneities, where $\omega_k = 2\sin(k/2)$ is the linear dispersion relation and $v_k = d\omega_k/dk = \cos(k/2)$ is the group velocity; the RHS of (1) is the 4–wave collision integral

$$\mathcal{I}_k = 4\pi \int_0^{2\pi} |T_{k123}|^2 n_k n_{k_1} n_{k_2} n_{k_3} \left(\frac{1}{n_k} + \frac{1}{n_{k_1}} \right.$$
$$\left. - \frac{1}{n_{k_2}} - \frac{1}{n_{k_3}} \right) \delta(\Delta K) \delta(\Delta \Omega) dk_1 dk_2 dk_3, \tag{2}$$

where the arguments of the Dirac's deltas are defined as $\Delta K = k + k_1 - k_2 - k_3$, $\Delta \Omega = \omega_k + \omega_1 - \omega_2 - \omega_3$, and $|T_{k123}|^2 = 9\omega_k \omega_1 \omega_2 \omega_3/16$ is the matrix element associated with the β–FPUT model [28, 32]. The integration of (2) has only one degree of freedom, since the resonance conditions imposed by the Delta functions constrain the integration to the so-called *resonant manifold*,

i.e. the subset of possible combinations of k_1, k_2, k_3 that are in resonance with mode k, representing all the resonant wave quartets. We provide an explicit expression of this one-dimensional integration in the *Materials and Methods* section.

The resonant interactions contained in the collision integral represent the mechanism responsible for the local (*i.e.* at fixed x) relaxation to the equilibrium distribution of n_k which, given the two conserved quantities of (1), is given by the Rayleigh-Jeans (RJ) solution

$$n_k^{(RJ)} = \frac{T}{\omega_k + \mu}. \tag{3}$$

Here, T plays the role of the temperature of the system and μ of the chemical potential; these quantities are associated with the conservation of the harmonic energy and of the action (or number of particles), respectively. The spatial energy density profile can be computed multiplying n_k by ω_k and integrating in k:

$$e(x, t) = \int_0^{2\pi} \omega_k n(x, k, t) dk. \tag{4}$$

To avoid confusion, we recall that due to the discreteness of the physical space the Fourier space is periodic and therefore the modes in the interval $[\pi, 2\pi)$ can be equivalently interpreted as in $[-\pi, 0)$. For this reason, hereafter we refer to the modes near 0 or 2π as the *low wavenumbers* and to the modes near π as the *high wavenumbers*.

RESULTS

In what follows, we will discuss results achieved from two types of numerical simulations of the nonhomogeneous wave kinetic equation: case (A) corresponds to the classical problem of a chain in between two thermostats at different temperatures and case (B) corresponds to the free evolution of an initial energy density narrow Gaussian profile in x. The latter is the typical experiment used to asses the diffusive (or not) properties of the system.

A. Anomalous conduction

To demonstrate numerically anomalous conduction, we consider a domain of size L with two thermostats at its ends at different temperature T_1 and T_2. For normal conduction, at the steady state one expects a linear temperature, T, profile (Fourier's law) and the conductivity, $\mathcal{K}$, to be independent of the size of the domain, L. By defining the net spectral energy current as

$$j(k, x, t) = \omega_k v_k [n(k, x, t) - n(-k, x, t)]/2, \tag{5}$$

the conductivity can be computed as

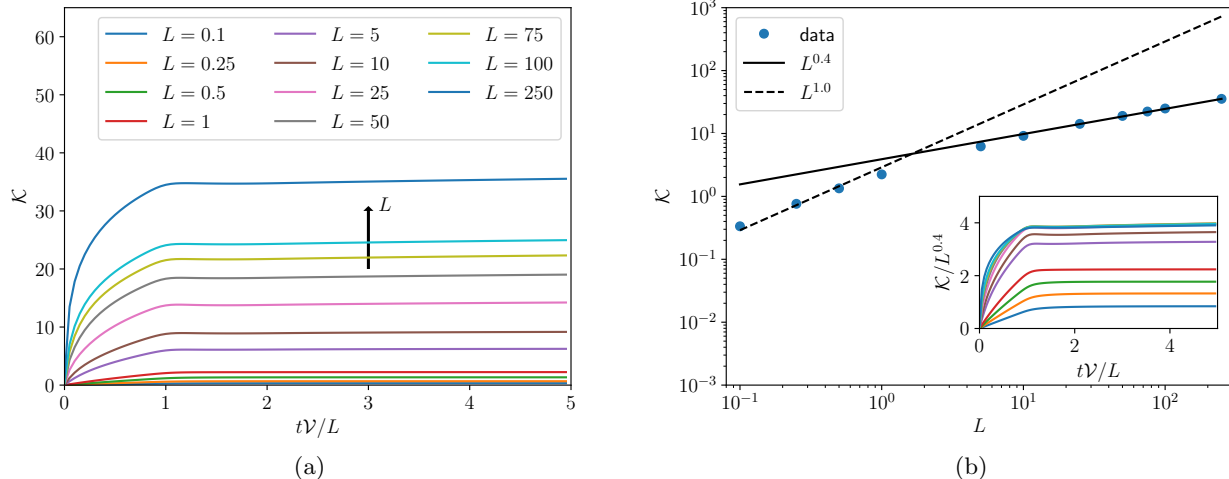$$\mathcal{K} = \frac{JL}{\Delta T} \tag{6}$$

FIG. 1: (a) Thermal conductivity $\mathcal{K}$ as function of non-dimensional time for several values of L; (b) Steady state thermal conductivity $\mathcal{K}$ as a function of L. For small L most of the modes are non-interacting and the ballistic scaling $\mathcal{K} \propto L^1$ is recovered. For larger L, we observe excellent asymptotic agreement with the scaling $\mathcal{K} \propto L^{0.4}$. The inset of panel (b) reports the thermal conductivity $\mathcal{K}$ in panel (a) normalized by $L^{0.4}$ as a function of non-dimensional time.

with

$$J = \frac{1}{L} \int_0^L \int_0^{2\pi} j(k,x,t) dk dx, \qquad (7)$$

being the spatial average of the integral of $j(k,x,t)$ and $\Delta T = T_1 - T_2$ the temperature difference between the two thermostats. The term $\Delta T/L$ represents the mean temperature gradient and one can recognize the definition of $\mathcal{K}$ as given by Fourier's law. Note that, at the steady state, the energy current is independent of x.

In Fig. 1a, we report the time history of the conductivity for several values of the domain size L, keeping fixed ΔT. The initial ($t = 0$) distribution is set to be a RJ distribution at the average temperature between the two thermostats; subsequently, there is an initial transient during which the energy flux starts growing (and consequently also $\mathcal{K}$), until a stationary state is reached. Note that time is made non-dimensional with the reference time $L/\mathcal{V}$, with $\mathcal{V} = v_{k=0} = 1$ being the maximal ballistic velocity. In Fig. 1b, instead, we report the measured conductivity as a function of the domain size L: the results clearly indicate that for small L the stationary value of the conductivity tends to be proportional to L, as in the purely harmonic system; on the other hand, for $L \to \infty$ the exponent α tends to the constant value of 0.4, consistent with the value measured in the microscopic simulations [25]. In the inset of the figure, the time history of the conductivity $\mathcal{K}$ divided by $L^{0.4}$ is drawn to highlight that for large values of L the curves overlap.

Via integration of the deterministic microscopic equations, a recent work [29] provided evidence that the collision integral $\mathcal{I}_k$ brings the system to local equilibrium down to a critical k_c whereas, for lower k's advection is

predominant and waves travel in the domain transported by the group velocity v_k interacting too weakly in order to relax locally to a RJ spectrum. Here, we observe this clearly by looking at the evolution of the color map of the temperature in Fig. 2, where the temperature spectral density $T(x,k,t) = (\omega_k + \mu) n(x,k,t)$ is defined by inverting (3), using the fact that μ is constant throughout the evolution. Note that for $k < \pi$ the velocity v_k is positive, while it is negative for $k > \pi$. The initial condition at $t = 0$ is a homogeneous field, with $n(x,k,t = 0) = n_k^{(RJ)}$ at temperature $(T_1 + T_2)/2$. Due to the presence of the thermostats, as $t > 0$ the waves going to the right start to propagate a hot front from the left thermostat, while the waves going to the left start propagating a cold front from the right thermostat. The edge of the front propagates at the maximal speed allowed, which is the speed of the acoustic modes $v(k \to 0^\pm) = \pm 1$. For $L = 1$, the energy flows in a ballistic way for almost the entire domain and the collision integral is not strong enough to bring the system to local equilibrium. As a result, at large times and at any fixed point x, the right-going waves are at temperature T_1 and the left-going waves are at temperature T_2, far from local equipartition. For larger system size, $L = 10$, instead, advection is predominant only in a small range of k, with the remaining part of the domain dominated by diffusion: in this region, at large time and at any fixed point x, the energetic content of the left- and right-going waves is equipartitioned, and there is a constant smooth temperature gradient between the two thermostats. This is reflected in the profile in k of the spatial integral of the spectral energy current $\langle j \rangle_x = \frac{1}{L} \int_x j(k,x) dx$, once a steady state is reached, see
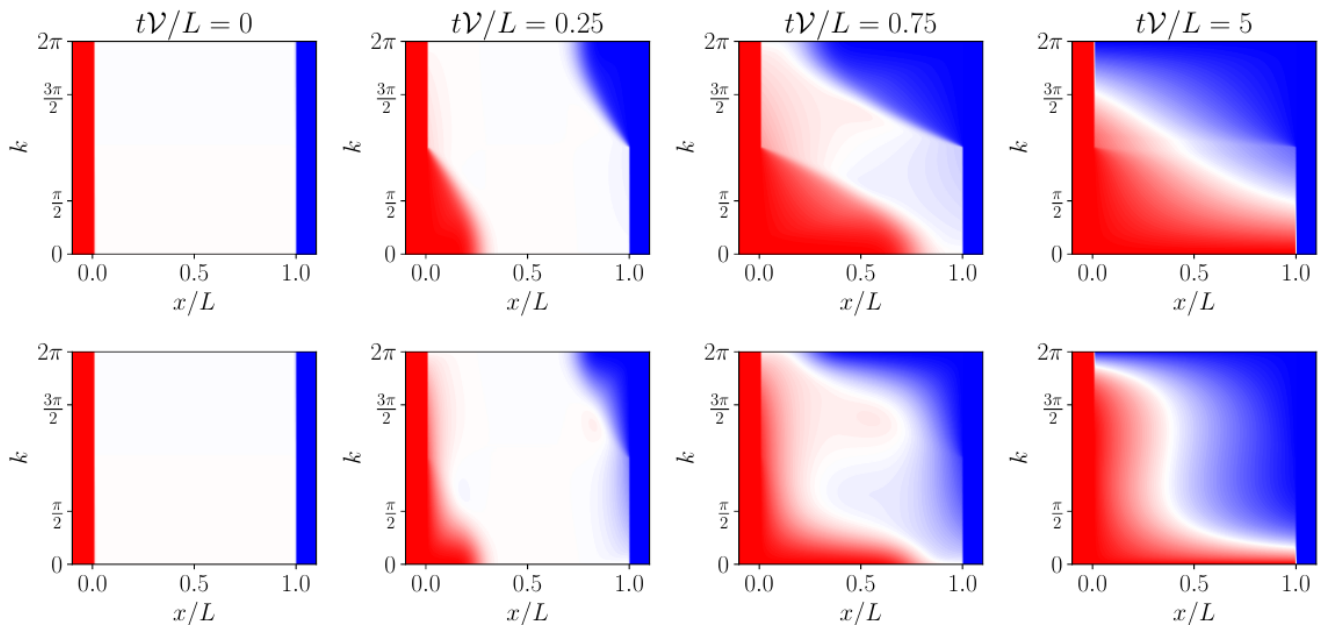
FIG. 2: Color map of $T(x, k, t) = (\omega_k + \mu)n(x, k, t)$. Top row: $L = 1$; bottom row: $L = 10$. Color ranges from T_2 (white) to T_1 (red). For $t > 0$, two fronts start propagating the temperature of the thermostats, perturbing the initial homogeneous state. The modes in $[0, \pi]$ propagate to the right ($v_k > 0$) and the modes in $[\pi, 2\pi]$ propagate to the left ($v_k < 0$). The upper panels depict a predominantly ballistic situation also at the stationary state (right panel), since L is not sufficiently large for most of the modes to interact. For the larger system in the lower panels, once a steady state is reached the diffusive modes (around $k = \pi$) have equipartitioned at fixed x and are accompanied by a $k-$independent constant gradient between the two thermostats. On the other hand, the ballistic modes (around $k = 0$ and $k = 2\pi$) carry the energy density of their originating thermostat all the way to the opposite side without interactions with other modes. Here we observe that the width of the ballistic region becomes thinner as L increases (see Fig. 4).

figure 3a. For modes with small k, $\langle j \rangle_x$ is independent of the system size since the behavior is purely ballistic [3]. For modes with large k the energy current flattens as L increases, accompanied by a reduction of the peak value. In particular, Fig. 3b shows how for these modes the energy current is in inverse proportionality with the chain length L as one would expect from Fourier's law, i.e. (6) when $\mathcal{K}$ does not depend on L. There shoud be, then, a critical value k_c above which the evolution of the energy is diffusion-dominated and below which the predominant transport mechanism is the purely ballistic one. Considering that at equilibrium the transport term and the collision integral should balance, and using dimensional arguments, one can find that $k_c \approx L^{-3/10}$ [29]. A scaling consistent with this estimation can be found, in our simulations, for the value of k for which $\langle j \rangle_x$ is maximal, as reported in figure 4, suggesting that this criterion could be used as a proxi for the determination of $k_c(L)$, to distinguish between diffusive and ballistic modes.

B. Ballistic and diffusive propagation

In nonequilibrium statistical physics, the transport coefficients characterizing nonequilibrium steady states

that are not too far from equilibrium can be computed in terms of space-time correlations in an equilibrium ensemble of realizations of the microscopic dynamics [2, 5, 27, 33, 34], via the so-called Kubo integral. Likewise, for the mesoscopic model of (1), let us now consider an initial background equilibrium state with constant $T = T_0$ and chemical potential μ. Let us then consider an initial narrow bell-shaped perturbation $\delta T(x)$ in the center of the domain, such that $\delta T \ll T_0$. We initialize $n(x, k, t = 0)$ with a RJ distribution, see (3), with $T(x) = T_0 + \delta T(x)$, in a domain going from $-L$ to L.

The evolution of $\langle n \rangle_k(x, t) = \int_0^{2\pi} n(x, k, t)dk$ is shown in Fig. 5, where we considered a perturbation having an initial amplitude of $\delta T(x = 0)/T_0 = 0.1$. One can recognize the familiar behavior of a central peak (*heat peak*) and two traveling peaks (*acoustic peaks*) which correspond to the emission of the *second sound*. This configuration has been studied using the the microscopic dynamics [5, 33] and the stochastic model known as *fluctuating hydrodynamics* [34]. For $t > 0$, two peaks separate and propagate in opposite directions with constant velocity about ± 1; the central peak, instead, evolves diffusively in time (Fig. 5a). This is clearly visible by looking at the time evolution of the variance of the distribution, com-
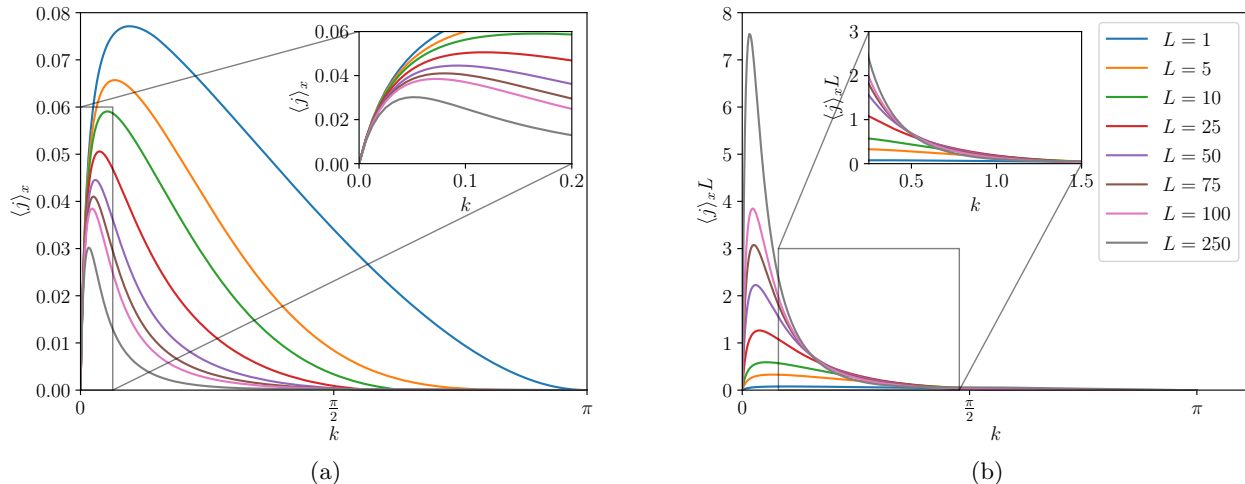
(a)

(b)

FIG. 3: (a) Energy current $\langle j \rangle_x$ as function of k for different domain size, once a steady state has been reached. While for the high wavenumbers the energy current contribution decreases as L increases, the low-wavenumber contribution is independent of L, in agreement with a ballistic behavior. In the inset, one can appreciate this invariance as $k \to 0$. (b) The energy current $\langle j \rangle_x$ is multiplied by the size of the domain L. Now, the renormalized curves tend to converge onto each other independently of L for the high wavenumbers. This behavior is in agreement with Fourier's law (see (6)) prescribing inverse proportionality between energy current and system size.
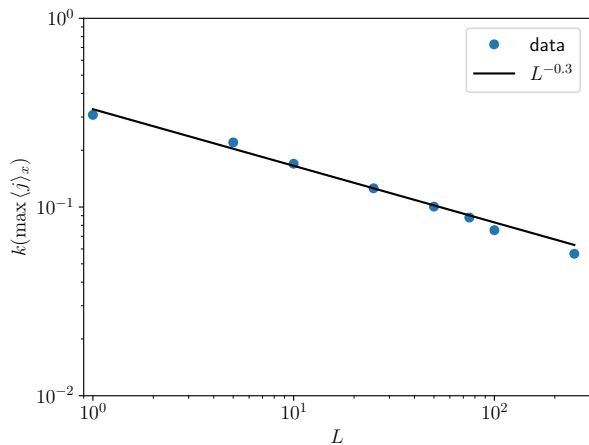

FIG. 4: Scaling of $k(\max(\langle j \rangle_x))$ (defined as the point of maximum in Fig. 3a) as function of L. The observed scaling is consistent with $L^{-0.3}$, which implies an anomalous exponent $\alpha = 0.4$.

puted as follows:

$$\sigma^2 = \frac{\int_{x,k} n(k,x,t)\omega(k)x^2 dx dk}{\int_{x,k} n(k,x,t)\omega(k) dx dk}. \tag{8}$$

Indeed, as shown in Fig. 5b, after the acoustic peaks exit the domain (at about $t\mathcal{V}/L = 1$) and the central peak is left alone, the variance starts to grow linearly in time. The time evolution of the central peak follows regular

diffusion, with diffusion coefficient given by half the slope of the asymptote on the right hand-side of Fig. 5b. This particular result may sound controversial in the face of notable results advocating for a *heat peak* that follows *fractional diffusion* (of super-diffusive type). We address this further in the *Discussion* section.

We can therefore identify the second sound emission with the non-decaying transport of the ballistic modes, and the *heat peak* with the regular diffusion of the modes that thermalize locally. Further confirmation of this is found in Fig. 6, where we plot the time evolution of the small initial Gaussian perturbation on homogeneous background, and we show that the numerical simulation of the WKE follows closely a diffusive solution with diffusion coefficients around 0.24, for this condition. Thus, we can simply refer to the *heat* and the *acoustic* peaks as to the *diffusive* and the *ballistic* (or *second-sound*) peaks, respectively, without ambiguity. Fig. 7 shows the energy density $e(x,k,t)$ at various times of the evolution of the perturbation. The low modes, with $k \approx 0$ and $k \approx 2\pi$, are the ones with the highest ballistic velocity. Hence, they will leave the domain in a timescale of the order of $L/\mathcal{V}$. For longer times, the higher modes start to diffuse thanks to the collision integral and the distribution will start to follow a diffusive evolution.

DISCUSSION

Our direct numerical simulation of the WKE shows that two phononic states coexist in the β-FPUT chain. The first, involving the low modes, is equivalent to the
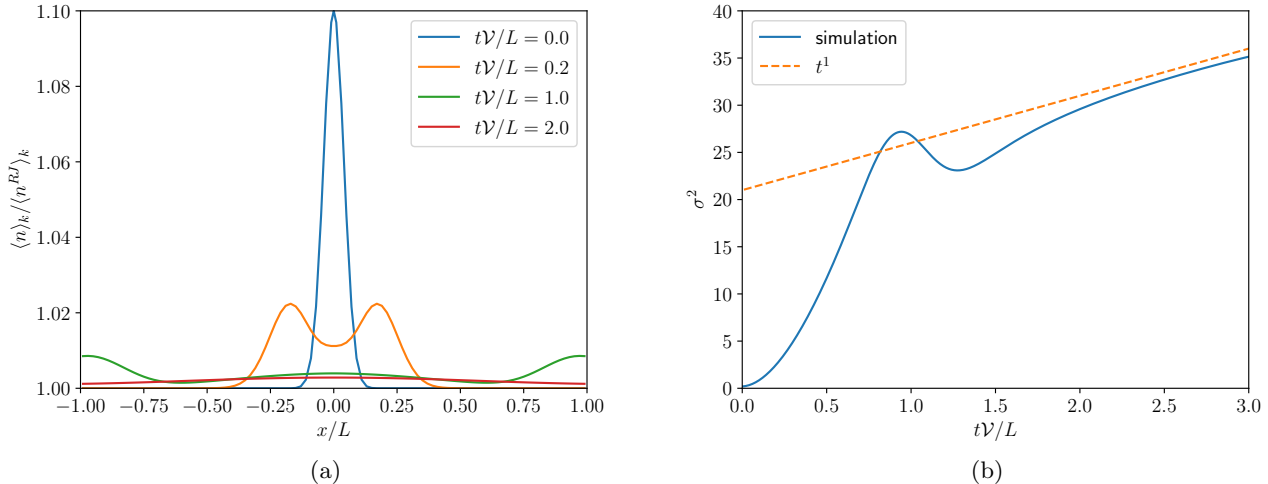
FIG. 5: (a) Spatial distribution of $\langle n \rangle_k(x,t)$ (integrated in k) at different times. An initial spatially localized perturbation over a uniform background propagates as two ballistic peaks moving in opposite direction at constant velocity and a central decaying peak. (b) Time history of the variance of the temperature distribution. After the ballistic peaks exit the system, the broadening of the central peak (also known as the heat peak) shows agreement with a diffusive behavior.
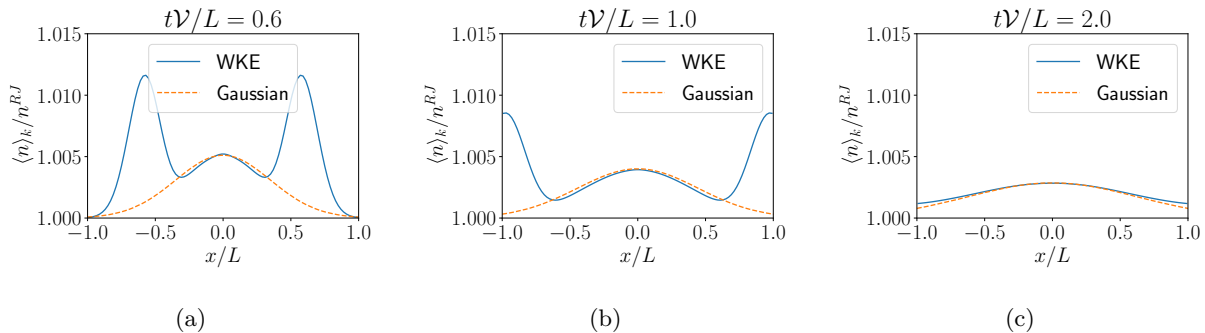

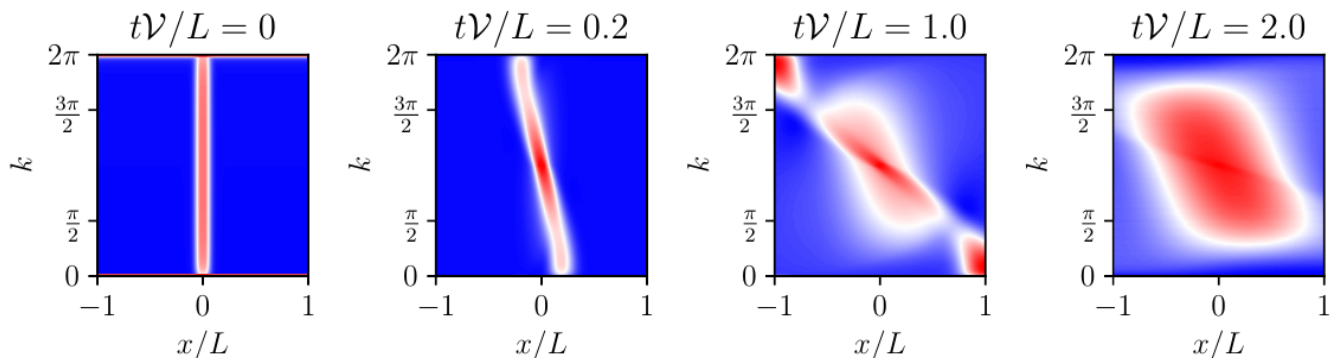FIG. 6: Heat peak evolution as predicted by WKE (–), and pure diffusion (- -).

FIG. 7: Color map of $e(x,k,t) = \omega_k n(x,k,t)$ at four non-dimensional time instants. The second sound emission is clearly seen in the central maps where perturbations at $k \simeq 0$ and $k \simeq 2\pi$ (the low modes) are detaching from the central diffusive peak involving the high modes. The interacting and diffusive character of these modes is evident from the fact that the shape of the central peak remains close to a rectangle during the evolution, tending to populate all modes k with the same energy density at fixed position x.

emission of second sound; the second, involving the higher modes, is purely diffusive. This has been analyzed under the following different points of view.

- The anomalous scaling of the energy conductivity $\mathcal{K} \propto L^\alpha$, with $\alpha \simeq 0.4$, is confirmed in Figs. 1a-1b. This is due to the scaling $k_c(L)$ of the separation between the ballistic modes (low wavenumbers) and the diffusive modes (high wavenumbers), individually contributing towards $\alpha = 1$ and $\alpha = 0$, respectively. We find that k_c varies consistently with L by the scaling $k_c(L) \propto L^{-3/10}$, as shown in Fig. 4.

- The spatial integral of the spectral energy current modal density $\langle j \rangle_x(k)$ is independent of L for the low modes, as predicted for the purely harmonic chain [3], while it is proportional to L^{-1} for the higher modes, in agreement with Fourier's law. This was shown in Fig. 3.

- A complementary way to analyze energy transport is to look at the evolution of a small localized perturbation of the thermal equilibrium condition. By doing that, we confirm the presence of two *acoustic* peaks shooting off in opposite directions and a central *heat* peak (figure 5a) evolving in agreement with standard Fourier diffusion, as confirmed in Figs. 5b and 6a-6c.

- Existence of the two types of heat transfer, ballistic and diffusive, is cleanly demonstrated in Figs. 2 and 7. In Fig. 2 the qualitative difference between these two types is most evident near the stationary nonequilibrium state, where the horizontal separation between the two different regions gives an intuitive visualization of k_c. Finally, in Fig. 7 we see an $x - k$ representation of the evolution of a perturbed equilibrium state. Again, the sharp separation wavenumber, k_c, can be observed by eye. Not surprisingly, we discover that the acoustic peaks are made exclusively of noninteracting ballistic modes with low wavenumber, while the heat peak is made exclusively of modes with high wavenumber.

Although the separation of scales at k_c observed in the $x - k$ plots is slightly smeared, the two-state ballistic-diffusive picture analyzed above under these four different angles is robust and does not include super-diffusive propagation with fractionary exponents. A fractionary diffusion equation with space derivative of order 8/5 instead of 2, is an alternative explanation compatible with the conductivity scaling $K \propto L^{2/5}$, rigorously derived in [35]. However, this scaling would predict the propagation of a single peak that does not find correspondence in our observations. The apparent disagreement may have different origins. For example, the assumption of having only two conserved quantities (energy and action) made in [35] is partially violated by the ballistic modes, which effectively preserve momentum and whose propagation

is not a part of the heat peak. Although we have assessed overall compatibility of the heat peak evolution with a diffusive behavior, providing a definitive study of this issue is not the aim of the current manuscript. In close analogy with *second sound* propagation in superfluids [36], our results show that, if the ballistic phonons are recognized as noninteracting traveling waves [29, 37, 38], the two-state ballistic-diffusive picture is compatible with the main observable aspects of energy transport.

Finally, it is worth noticing that second sound in dielectric solids was predicted a long time ago [39–41], and later observed for instance in solid He^3 and He^4 below 4 K and in NaF below 20 K, at extremely low temperature. In a dielectric crystal, second sound can be observed when Umklapp resonances are very small, and by lowering the temperature enough, the scattering level is reduced to a point where noninteracting wavelike transport becomes visible on macroscopic scales. It is now well-known that reducing the dimensionality of the material is another way to reduce drastically the number of interactions, in part explaining why it was recently possible to observe second-sound propagation in 2D graphite at temperatures above 100 K [42, 43]. Our results further indicate that reducing the dimensionalty to (quasi-)1D structures such as nanotubes may give a hope to finally observe second-sound propagation at room temperature.

MATERIALS AND METHODS

Integration on the resonant manifold

In (2), the equality coming from the momenta Dirac delta has to be interpreted mod I, $I = [0, 2\pi)$, to include possible Umklap resonances. The resonant manifold is the subset of $I \times I \times I \times I$ satisfying at the same time the two conditions

$$\omega_k + \omega_{k_1} - \omega_{k_2} - \omega_{k_3} = 0, \qquad k_3 = (k + k_1 - k_2) \mod I. \quad (9)$$

The constraint imposed by integration on the resonant manifold reduces the triple integral of (2) to a one-dimensional integral. Here, we briefly report some important rigorous results from Ref. [28] (see also [26, 33]). The solutions of the collisional constraints (9) are of three types:

- $k_1 = k_3, k_2 = k_4$;

- $k_1 = k_4, k_2 = k_3$;

- $k_2 = h(k_1, k_3) \mod I$, where

$$h(x, y) = \frac{y - x}{2} + 2 \arcsin\left(\tan \frac{|y - x|}{4} \cos \frac{y + x}{4}\right). \quad (10)$$

The first two types (perturbative solutions) are trivial resonances that contribute to nonlinear frequency shift and broadening [24]. The third type of solutions (non-perturbative) represents non-trivial resonances that are responsible for irreversible spectral transfers. By integrating analytically in k_3, the collision integral of (2) can be written as

$$\mathcal{I}_k = \int_0^{2\pi} dk_1 dk_2 \, g(k, k_1, k_2) \delta(\Omega(k, k_1, k_2)), \qquad (11)$$

with

$$g(k, k_1, k_2) = |T_{k,k_1,k_2,k+k_1-k_2}|^2 n_k n_{k_1} n_{k_2} n_{k+k_1-k_2}$$
$$\times \left(\frac{1}{n_k} + \frac{1}{n_{k_1}} - \frac{1}{n_{k_2}} - \frac{1}{n_{k+k_1-k_2}} \right), \qquad (12)$$
$$\Omega(k, k_1, k_2) = \omega_k + \omega_{k_1} - \omega_{k_2} - \omega_{k+k_1-k_2}.$$

In order to integrate out the frequency delta, we exploit the following property of the Dirac delta function:

$$\int dx \, G(x) \delta(f(x)) = \int dx \, G(x) \sum_i \frac{\delta(x - x_i^\star)}{|f'(x_i^\star)|}, \qquad (13)$$

where $x_i^\star$ are all the zeros of f. In (11), integrating in the variable k_1, we know that all of the zeros of $\Omega = 2[\sin(k/2) + \sin(k_1/2) - \sin(k_2/2) - \sin(|k+k_1-k_2|/2)]$ are of one of the three types above. The trivial solutions give $\Omega'(k_1) = 0$ identically, which implies singlular denominators. Though, as discussed in Ref. [28] these terms come in pairs of opposite sign (this can be seen easily looking at the symmetries of the integrand of (2)), which cancel each other and do not contribute. Therefore, the non-vanishing contributions come from the non-

trivial resonances, and we obtain

$$\mathcal{I}_k = \int_0^{2\pi} dk_2 \int_0^{2\pi} dk_1 \, g(k, k_1, k_2) \frac{\delta(k_1 - h(k, k_2))}{|\partial_{k_1} \Omega(k, h(k, k_2), k_2)|}$$
$$= \int_0^{2\pi} dk_2 \, \frac{g(k, h(k, k_2), k_2)}{\sqrt{\left(\cos \frac{k}{2} + \cos \frac{k_2}{2} \right)^2 + 4 \sin \frac{k}{2} \sin \frac{k_2}{2}}} \cdot$$
$$(14)$$

Numerical details

(1) is solved by finite difference approximation in time and space, using the expression of $\mathcal{I}_k$ given in (14). In all simulations we used 100 grid points in x and 1001 points in k; the chemical potential is set to $\mu = 0.05$. The adopted discretization guarantees the conservation of energy and wave action. In *Case A* of the *Results* we used $T_1 = 0.4$, $T_2 = 0.2$. In *Case B* of the *Results* we used $T_0 = 0.3$, $\delta T(x = 0)/T_0 = 0.1$.

ACKNOWLEDGEMENTS

[1] J. B. J. baron de Fourier, Théorie analytique de la chaleur (Firmin Didot, 1822).

[2] R. Kubo, M. Toda, and N. Hashitsume, Statistical physics II: nonequilibrium statistical mechanics, Vol. 31 (Springer Science & Business Media, 2012).

[3] Z. Rieder, J. Lebowitz, and E. Lieb, Journal of Mathematical Physics **8**, 1073 (1967).

[4] A. Dhar and K. Saito, in Thermal Transport in Low Dimensions (Springer, 2016) pp. 39–105.

[5] S. Lepri, R. Livi, and A. Politi, Physics reports **377**, 1 (2003).

[6] D. Donadio and G. Galli, Physical review letters **102**, 195901 (2009).

[7] C.-W. Chang, D. Okawa, H. Garcia, A. Majumdar, and A. Zettl, Physical review letters **101**, 075903 (2008).

[8] J. Chen, G. Zhang, and B. Li, Nano letters **10**, 3978 (2010).

[9] S. Shen, A. Henry, J. Tong, R. Zheng, and G. Chen, Nature nanotechnology **5**, 251 (2010).

[10] N. Yang, G. Zhang, and B. Li, Nano Today **5**, 85 (2010).

[11] S. Liu, X. Xu, R. Xie, G. Zhang, and B. Li, The European Physical Journal B **85**, 337 (2012).

[12] C.-W. Chang, in Thermal Transport in Low Dimensions (Springer, 2016) pp. 305–338.

[13] S. Lepri, Thermal transport in low dimensions: from statistical physi Vol. 921 (Springer, 2016).

[14] E. Fermi, J. Pasta, and S. Ulam, Fermi, Collected Papers **2**, 977 (1955).

[15] G. Gallavotti, The Fermi-Pasta-Ulam problem: a status report, Vol. 728 (Springer, 2007).

[16] R. Peierls, Annalen der Physik **Vol. 3**, 1055–1100 (1929).

[17] V. E. Zakharov, V. S. L'vov, and G. Falkovich, Kolmogorov spectra of turbulence I: Wave turbulence (Springer Science & Business Media, 2012).

[18] Y. Choi, Y. V. Lvov, and S. Nazarenko, Physica D: Nonlinear Phenomena **201**, 121 (2005).

[19] S. Nazarenko, Wave turbulence, Vol. 825 (Springer Science & Business Media, 2011).

[20] G. L. Eyink and Y.-K. Shi, Physica D: Nonlinear Phenomena **241**, 1487 (2012).

[21] S. Chibbaro, G. Dematteis, C. Josserand, and L. Rondoni, Physical Review E **96**, 021101 (2017).

[22] S. Chibbaro, G. Dematteis, and L. Rondoni, Physica D: Nonlinear Phenomena **362**, 24 (2018).

[23] M. Onorato and G. Dematteis, Journal of Physics Communications **4**, 095016 (2020).

[24] Y. V. Lvov and M. Onorato, Physical review letters **120**, 144301 (2018).

[25] S. Lepri, R. Livi, and A. Politi, EPL (Europhysics Letters) **43**, 271 (1998).

[26] A. Pereverzev, Physical review E **68**, 056124 (2003).

[27] K. Aoki, J. Lukkarinen, and H. Spohn, Journal of statistical physics **124**, 1105 (2006).

[28] J. Lukkarinen and H. Spohn, Communications on Pure and Applied Mathematics: A Journal Issued by the Courant Institute of Mathematical Sciences **61**, 1753 (2008).

[29] G. Dematteis, L. Rondoni, D. Proment, F. De Vita, and M. Onorato, Phys. Rev. Lett. **125**, 024101 (2020).

[30] Y. Deng and Z. Hani, arXiv preprint arXiv:2104.11204 (2021).

[31] I. Ampatzoglou, C. Collot, and P. Germain, arXiv preprint arXiv:2107.11819 (2021).

[32] M. D. Bustamante, K. Hutchinson, Y. V. Lvov, and M. Onorato, Communications in Nonlinear Science and Numerical Simulation **73**, 437 (2019).

[33] J. Lukkarinen, in Thermal transport in low dimensions (Springer, 2016) pp. 159–214.

[34] H. Spohn, in Thermal transport in low dimensions (Springer, 2016) pp. 107–158.

[35] A. Mellet and S. Merino-Aceituno, Journal of Statistical Physics **160**, 583 (2015).

[36] V. Peshkov et al., Helium **4**, 166 (2013).

[37] V. A. Kuzkin and A. M. Krivtsov, Physical Review E **101**, 042209 (2020).

[38] V. A. Kuzkin and A. M. Krivtsov, Acta Mechanica **232**, 1983 (2021).

[39] M. Chester, Physical Review **131**, 2013 (1963).

[40] E. Prohofsky and J. Krumhansl, Physical Review **133**, A1403 (1964).

[41] D. Chandrasekharaiah, (1986).

[42] S. Huberman, R. A. Duncan, K. Chen, B. Song, V. Chiloyan, Z. Ding, A. A. Maznev, G. Chen, and K. A. Nelson, Science **364**, 375 (2019).

[43] G. Chen, Nature Reviews Physics **3**, 555 (2021).